Available online at www.sciencedirect.com

ScienceDirect

International Journal of Solids and Structures 44 (2007) 320–335

INTERNATIONAL JOURNAL OF SOLIDS and STRUCTURES

www.elsevier.com/locate/ijsolstr

Finite element modeling of porous titanium

H. Shen, L.C. Brinson *

Mechanical Engineering Department, Northwestern University, 2145 Sheridan Road, Evanston, IL 60208, USA

Received 19 July 2005; received in revised form 31 March 2006
Available online 27 April 2006

Abstract

The porous microstructures of metallic foams cause microscopic stress and strain localization under deformation which reduces the damage tolerance and therefore limits application of the materials. In this paper, the deformation of a relatively low porosity porous titanium is examined using two-dimensional (2D) plane strain and three-dimensional (3D) finite element models to identify the accuracy and limitations of such simulations. To generate the finite element models, a simulated microstructure was created based on micrographs of an experimental material. Compared to the 2D models, the 3D models require smaller model size to obtain convergent results. The macroscopic responses predicted by the 3D models are in reasonable agreement with experimental results while the 2D models underestimated the response. In addition, 3D models predicted more uniform microscopic field variable distributions. 2D models predicted higher probability of Von Mises stress and equivalent plastic strain exceeding a certain value and therefore overestimate the failure probability of the material.

Keywords: Porous titanium; Microstructure; Finite element analysis; Von Mises stress distribution; Plastic strain distribution

1. Introduction

Titanium-based foams inherit the excellent mechanical and biological properties of titanium and its alloys and have potential applications for structural materials and porous bone-replacement implants (Chang et al., 1996; Dunand, 2004; Wen et al., 2002a,b). In particular, as a potential implant material, stiffness of the porous material drops with the square of relative density to be comparable to bone stiffness and the open porosity allows bone ingrowth (Gibson and Ashby, 1997; Spoerke et al., in press). However, the porous microstructures of titanium foams cause stress and strain localization under deformation which reduces damage tolerance and therefore limits their application. Since the localization is governed by the microstructural configurations, it is necessary to be able to study the effect of pore morphology, porosity, and bone ingrowth on macroscopic and microscopic response with a model. Analytical models are capable of predicting the overall material response under greatly idealized conditions or simplifying assumptions (Benveniste, 1987; Gibson

* Corresponding author. Tel.: +1 847 467 2347; fax: +1 847 263 0540.
E-mail address: cbrinson@northwestern.edu (L.C. Brinson).

0020-7683/$ - see front matter
doi:10.1016/j.ijsolstr.2006.04.020

and Ashby, 1997; Ju and Tseng, 1996; Mori and Tanaka, 1973). In contrast, finite element (FE) models are able to provide a full field solution and are therefore needed to realistically represent the microstructure which is typically heterogeneous.

The porous titanium considered here was processed by a solid-state foaming technique which consists of two steps: first, individual high-pressure argon pores are created within a billet by densification of powders in the presence of argon gas; a second foaming step consists of expansion, by plastic deformation of the surrounding matrix of these individual pores at elevated temperature (Dunand, 2004; Murray and Dunand, 2003). When porosity is less than 25%, pores are mostly rounded, generally equiaxed, and un-merged, as illustrated in Fig. 1(a) (Murray and Dunand, 2003). As the material is foamed to high porosity, these initially-isolated pores coalesce to form large pores having a complex, tortuous shape as shown in Fig. 1(b). One target application for the Ti foams is as a bone implant material, in which the porous microstructure can provide reduced stiffness (for reduced stress-shielding) as well as sites for bone ingrowth (Spoerke et al., in press). To simultaneously maintain mechanical durability, a porosity of 40–50% is generally considered to be an ideal range for the orthopaedic application. In addition, in this porosity range, high open porosity can be achieved and percolated pores allow significant bone ingrowth (Murray and Dunand, 2003). However, the high contrast properties of the two phases (pores and matrix) make it very difficult to obtain a representative volume element (RVE) in FE simulation of foams (Bouyge et al., 2002, 2001; Jiang et al., 2001; Shen and Brinson, in press). At porosities over 30%, the RVE problem is further complicated by coalescence of pores complicating the microstructure (Shen and Brinson, in press). Therefore, for the purposes of this initial study on the relevance of 2D models for overall properties and localization behavior in porous titanium, we focus on a lower

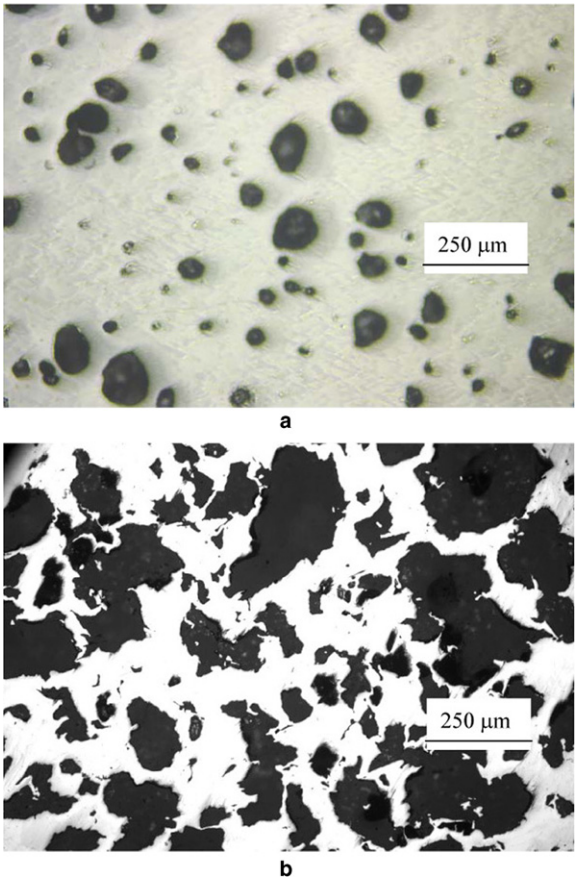

Fig. 1. Optical micrograph of metallographic cross-section for titanium foams with (a) 14.7% porosity and (b) 50% porosity.

porosity porous titanium and examine the more complex issues of high porosity in a later paper (Shen and Brinson, in preparation).

The microstructural geometry of a porous titanium at low porosity (14.7%) in Fig. 1(a) is similar to particle-reinforced metal matrix composites (PR MMCs) since their microstructures are both characterized by inclusions and matrix and the connectivity of inclusions is low. The FE approaches for PR MMCs can therefore be utilized for the analysis of low porosity porous titanium. For the numerical simulation of PR MMCs, to minimize computational requirements, it is often assumed that particles with one size are uniformly distributed in matrix regardless of local heterogeneity (Christman et al., 1989; Llorca et al., 1991; Song et al., 1996; Weissenbek et al., 1994). Based on this assumption, unit cell models containing a single particle are used, reducing the microstructure to a single repetitive building block. For the same reason, although the microstructures are strongly three-dimensional (3D), two-dimensional (2D) multi-particle models have also been widely used to study the local stress and strain distribution while taking into account the distribution of particles (Ghosh et al., 1996; Ramakrishnan et al., 1996; Wang et al., 1993; Wolodko et al., 2000).

The validity of simplifying a 3D microstructure to unit cell or 2D multi-particle models has been explored by some researchers by conducting the comparison among these three types of models (Bohm et al., 2002; Bohm and Han, 2001; Lissenden and Shen, 2001; Shen and Lissenden, 2002, 2005). For microscopic response predictions, many differences have been found among these three types of models. For example, the maximum values of the stress and strain fields in a 3D multi-particle model with randomly distributed particles are much higher than the corresponding values in a unit cell model and the strain and stress localizations occur in the regions where particles are closely spaced. The plastic strain distributions predicted by 2D models are localized into bands inclined at 45° from the loading direction while 3D model predictions only show the localization around particles and no clearly net-worked plastic strain bands (Shen and Lissenden, 2002). For macroscopic response predictions, however, the uniaxial stress–strain responses predicted by the 2D multi-particle model under generalized plane strain condition and the unit cell model agree well with the prediction from the 3D multi-particle model (Shen and Lissenden, 2002).

Despite the similarity in microstructural geometry between PR MMCs and porous titanium, their failure mechanisms are different. While particles are added to the metal matrix in PR MMCs for reinforcement, the titanium matrix is weakened by pores in porous titanium. In PR MMCs, the hard and brittle reinforcements provide preferential sites for void nucleation by particle fracture leading to the ductile fracture of the matrix. In porous titanium, the inclusions are voids which have zero modulus and the concern for failure is the extensive plastic yielding and ductile fracture of pore walls caused by stress and strain localization in the matrix. The use of 2D FE analyses is attractive to help screen or design possible pore morphologies and distributions based on relatively simple FE models created to reproduce actual microstructures observed by metallographic sectioning. For example, 2D FE models were used by Li et al. to study the influence of the pore morphology on mechanical responses of porous titanium (Li et al., 2004). While utilizing 2D models to simulate 2D foams such as honeycomb cellular material seems reasonable (Simone and Gibson, 1998), the validity of simplifying the obviously 3D microstructure of the titanium foam to 2D multi-pore models needs to be explored by observing the correlation and difference between 2D and 3D FE analyses.

Unit cell models for porous materials usually simulate ligaments and pore walls of one pore which are similar to the models for cellular mechanics based on beam theory (Gibson and Ashby, 1997). Sihn and Roy (2004) characterized representative 3D idealized cell ligaments to correlate the microstructure of open-cell carbon foams with bulk properties (Sihn and Roy, 2004). A similar ligament cell model was developed to study the uniaxial compression behavior of regular shaped cellular metals by Ochsner and Lamprecht (2003). The predictions for the overall properties are in good agreement with experimental results. However, these models are only suitable for open-cell foams with high porosities, typically above 70%, since high porosity makes the ligaments relatively regularly distributed. For our target materials, the porosity is usually below 50% with isolated pores of various sizes randomly distributed and often small pores coexist with large pores as shown in Fig. 1.

In this paper, a simulated microstructure (a 4000 μm cube) has been created based on an experimental material with 14.7% porosity. 2D and 3D FE models were created by excising sections of the simulated microstructure. The uniaxial stress–strain response was simulated and compared with experimental measurements. The macroscopic and microscopic responses were evaluated to quantify the difference and correlation between

the 2D and 3D models. In addition, the convergence trend of the individual estimates by 2D and 3D models was discussed to shed light on the RVE for the numerical simulation of porous materials.

2. Finite element modeling

A 3D simulated microstructure was developed using the methodology presented in our previous work (Shen et al., 2006). In the microstructure (3D-MP-70271), 70,271 spherical pores were randomly located in a 4000 μm cube, providing 14.7% porosity. No pore impingement was permitted. The pore size distribution followed Weibull distribution of which the density function is denoted by $f(x)$ as follows (Tobias and Trindade, 1995):

$$f(x) = \frac{m}{x}\left(\frac{x}{c}\right)^{m} \mathrm{e}^{-(x/c)^{m}} \tag{1}$$

where the parameters, m and c, are shape and scale parameter, respectively. $m = 2.47$ and $c = 64.68$ were obtained for the pore sections observed in 2D sectioning planes providing average 2D pore diameter of 63.3 μm; based on a stereological analysis, 3D pore size distribution was determined leading to $m = 2.29$ and $c = 60.52$ and providing a 3D average pore diameter of 53.6 μm.

The simulated microstructure is comprised of two distinct phases, pores and titanium matrix. It was assumed that pores were linear elastic with a very low modulus of 10^{-7} GPa and Poisson's ratio of 0.3. Pores were meshed to avoid possible computational difficulties. In addition, models with low modulus mesh or without mesh in pores were compared and no difference was found in either microscopic or macroscopic prediction. The titanium matrix having elastic modulus of 110 GPa, Poisson's ratio of 0.33, and yield strength of 275 MPa is representative of CP Ti-40 (ASM International, 2002). The matrix yield surface follows the Von Mises yield criterion with isotropic hardening. All material properties and model simulations are for room temperature.

2D and 3D FE models were created by cutting planar sections or small cubic domains from the simulated microstructure. The boundary conditions for the 3D models under uniaxial compressive loading along x_2 direction are shown in Table 1. The front, back, left, and right faces of the model were constrained to remain planar and normal to one of the coordinate axes throughout the computations. Similarly, to simulate uniaxial compressive loading condition along x_1 or x_3 directions, a negative displacement is applied on the right or front surface of the 3D models while the faces parallel to loading directions remain planar. Therefore, the boundary conditions can be considered as periodic mechanically, but not microstructurally. Note that the "full" microstructural periodic BC requires the pores on opposing edges to be continuous and the faces are

Table 1
Boundary conditions

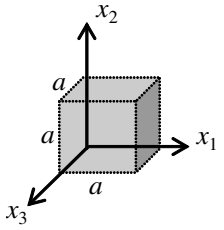

Model face	Boundary conditions
Right	$u_1 = -\bar{u}_1$
Left	$u_1 = \bar{u}_1$
Top	$u_2 = -0.01a$
Bottom	$u_2 = 0$
Front	$u_3 = -\bar{u}_3$
Back	$u_3 = \bar{u}_3$

$\bar{u}_1$ and $\bar{u}_3$ are displacements of the four side faces upon loading on the top.

not required to remain planar, but opposite pairs of faces are constrained to have compatible deformations. This unnatural microstructural periodicity is not applicable for the FE models developed by cutting out fragments of actual microstructures or simulated microstructures based on actual microstructures as in current research work. The boundaries for 2D models are the same as those applied to the left, right, top, and bottom faces of the 3D models to impose uniaxial compressive loading. Note that 2D models are restricted to uniaxial and biaxial load cases. All FE analyses are performed using the ABAQUS software with modified ten-node tetrahedral elements with hourglass control (C3D10M) for 3D analysis and eight-node biquadratic plane strain elements (CPE8) for 2D analysis (Hibbitt Karlsson Sorensen Inc., 2004). Mesh convergence was verified based on overall and local stress values. The overall strain and stress are calculated by using volume averages,

$$\bar{\varepsilon}_{ij} = \frac{1}{V}\int_V \varepsilon_{ij}\,\mathrm{d}V = \frac{1}{\sum_{m=1}^{N} V^{(m)}}\sum_{m=1}^{N} \varepsilon_{ij}^{(m)} V^{(m)} \tag{2}$$

$$\bar{\sigma}_{ij} = \frac{1}{V}\int_V \sigma_{ij}\,\mathrm{d}V = \frac{1}{\sum_{m=1}^{N} V^{(m)}}\sum_{m=1}^{N} \sigma_{ij}^{(m)} V^{(m)} \tag{3}$$

and the standard deviation of the microscopic stress distribution is weighted by the volume of the element

$$\mathrm{SD}_{ij} = \sqrt{\frac{\sum_{m=1}^{N} V^{(m)}\left(\sigma_{ij}^{(m)} - \bar{\sigma}_{ij}\right)^2}{\sum_{m=1}^{N} V^{(m)}}} \tag{4}$$

where $V^{(m)}$ is the volume of element m, N is the total number of elements, σ_{ij} is the Cauchy stress component, and the total strain component is decomposed into elastic and plastic components, $\varepsilon_{ij} = \varepsilon_{ij}^{\mathrm{E}} + \varepsilon_{ij}^{\mathrm{P}}$. It should be noted that the stress and strain components, σ_{ij} and ε_{ij}, are obtained at the centroid of each element. For 2D element (CPE8) in ABAQUS, element output variables are obtained at a centroidal integration point. For the 3D tetrahedral element C3D10M, element output variables are obtained by interpolation of the integration point values since the integration scheme for the element does not include a centroidal integration point.

2.1. 3D multi-pore finite element models

Four 3D models with porosity of 14.7% and side length of 340 μm were chosen from different locations of the 3D-MP-70271 microstructure, making the ratio of the model size to the average pore section size 6.34. The 3D models are named 3D-340 and one of the models is shown in Fig. 2. Some pores having a centroid near a face were truncated. The 3D model contains 64 pores and 125,536 elements on average.

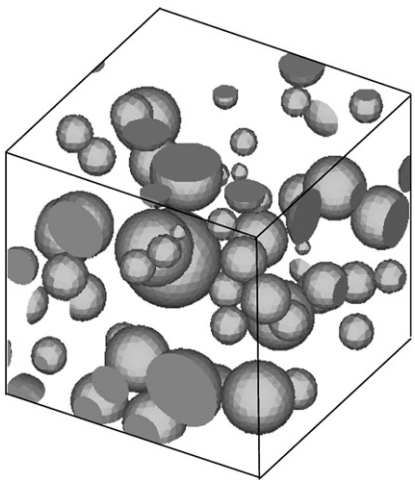

Fig. 2. Geometry of one 3D-340 model.

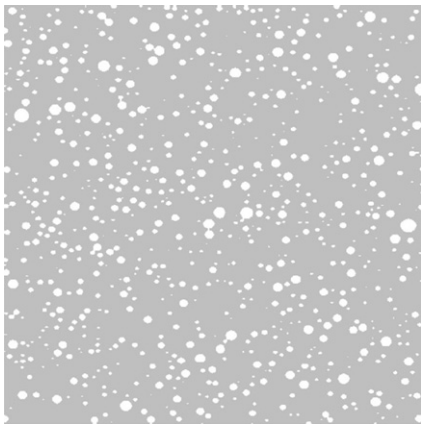

Fig. 3. Geometry of one 2D-4000 model.

2.2. 2D multi-pore finite element models

2D FE models are sometimes used since the size of 3D models causes long run times (Daxner et al., 2000; Li et al., 2004; Thelen et al., 2004). Eight 2D FE models with side length of 4000 μm were extracted from the sections in the 3D-MP-70271 microstructure, making the ratio of the model length to the average pore size 63.2. The area fraction of the 2D models matches the overall porosity of 14.7% and one of the models is shown in Fig. 3. The models were named 2D-4000. It can be seen that some pores having a centroid near an edge were truncated. There are 943 pores and 159,768 elements in each 2D-4000 model on average.

To compare 2D models with 3D models at the same length scale, one of the 3D-340 models was cut every 10 μm along x_3 axis to obtained planar sections parallel to the x_1x_2 plane. The area fractions of these smaller 2D sections ranged from approximately 4.4% to 29.2%. 2D models have been constructed for the section with the minimum area fraction (4.4%), called 2D-340-MIN; for the three sections with the area fraction equal to the porosity (14.7%), called 2D-340-MID; and for the section with the maximum area fraction (29.2%), called 2D-340-MAX. There are 6 pores and 3451 elements in the 2D-340-MIN model, 7 pores and 1508 elements in each 2D-340-MID model on average, and 10 pores and 1404 elements in the 2D-340-MAX model. The microstructures of the 2D-340-MIN, one of the 2D-340-MID, and the 2D-340-MAX models are shown in Fig. 4. All the 2D FE analyses are under plane strain condition.

3. Results and discussion

3.1. Macroscopic response

The uniaxial stress–strain responses predicted by the 2D and 3D models are shown in Fig. 5(a). There are six individual simulations (three models deformed along x_1 and x_2 directions) for the 2D-340-MID models, sixteen individual simulations (eight models deformed along x_1 and x_2 directions) for the 2D-4000 models; and twelve individual simulations (four models deformed along x_1, x_2, and x_3 directions) for the 3D-340 models. The average responses for each model group are shown in Fig. 5(b). The response of solid CP-Ti is shown for reference, from which the hardening behavior of the matrix material for FE calculation is obtained. The predicted elastic moduli, 0.2% offset yield strengths, and overall stresses at 1% far field strain are listed in Table 2 in terms of overall averages $\pm$ standard deviations and the maximum differences between the individual responses for all the 2D and 3D simulations. These collected results reveal that for the 2D-4000 and 3D-340 models, the individual predictions of the elastoplastic responses are within small ranges. For example, the range of overall stress predictions at 1% far field strain is 4.3% for the 2D-4000 models and 2.9% for the 3D-340 models. In our companion paper we demonstrate that the 2D-4000 and 3D-340 models are close to the 2D and 3D RVE sizes required for convergence (Shen and Brinson, in press). An approach to determine RVEs of porous titanium has been presented in that paper. The convergence of both the macroscopic and the

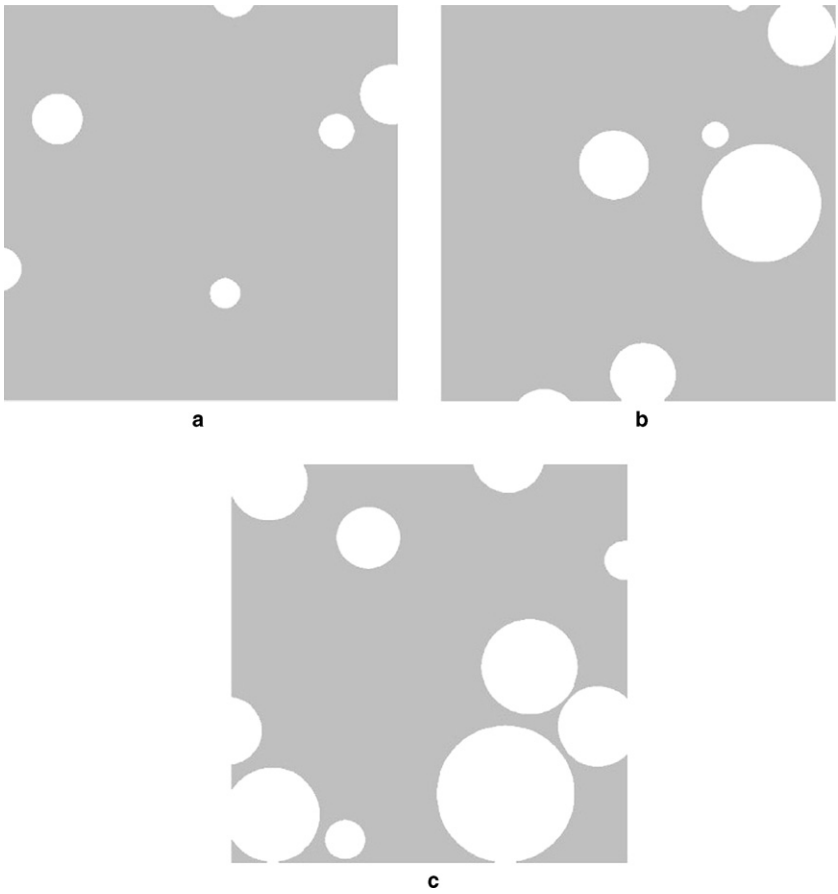

Fig. 4. Geometry of (a) 2D-340-MIN model, (b) one 2D-340-MID model, and (c) 2D-340-MAX model.

microscopic elastoplastic responses associated with the boundary conditions has been demonstrated. The nature of the discrepancy between these converged results is discussed below.

It is noteworthy that the stress–strain curves for the 2D-340-MID simulations are widely dispersed although their model length is equal to the 3D-340 models. The average response of the 2D-340-MID models is higher than that of the 2D-4000 models because models smaller than RVEs produce biased predictions. As the model size increases, the predictions converge to the RVE solution with small variation of results (Hazanov, 1999; Huet, 1990; Jiang et al., 2001; Shen and Brinson, in press). The observations above imply that the RVE size of the 3D simulation can be smaller than the 2D simulation.

The predictions from the 3D models are higher than the 2D models. The predicted elastic modulus, 0.2% offset yield strength, and overall stress at 1% far-field strain by the 3D-340 models are 4.38%, 17.83%, and 15.5% higher than those of the 2D-4000 models. This apparent higher strength in the 3D porous material is contrary with the observations on the simulation of PR MMCs that 2D plane strain models predict stronger plastic response than 3D models (Bohm and Han, 2001; Lissenden and Shen, 2001). For porous materials, since the 2D plane strain models implicitly assume continuous long pores through the thickness of the sample, the 3D models which account for the finite extent of the pores and the reinforcing matrix outside of the plane should indeed provide higher (and more accurate) mechanical response predictions. Although not shown here, the predictions from the 2D models under generalized plane strain or plane stress conditions are even lower than the plane strain results shown.

To verify the results predicted by the FE models, a compressive experiment was performed on a specimen of porous titanium (with rectangular cross-section of $4.7\,\text{mm} \times 4.6\,\text{mm}$ and height of 9.0 mm) with approximately 15% porosity and the experimental stress–strain curve is shown in Fig. 5(b) for comparison with the

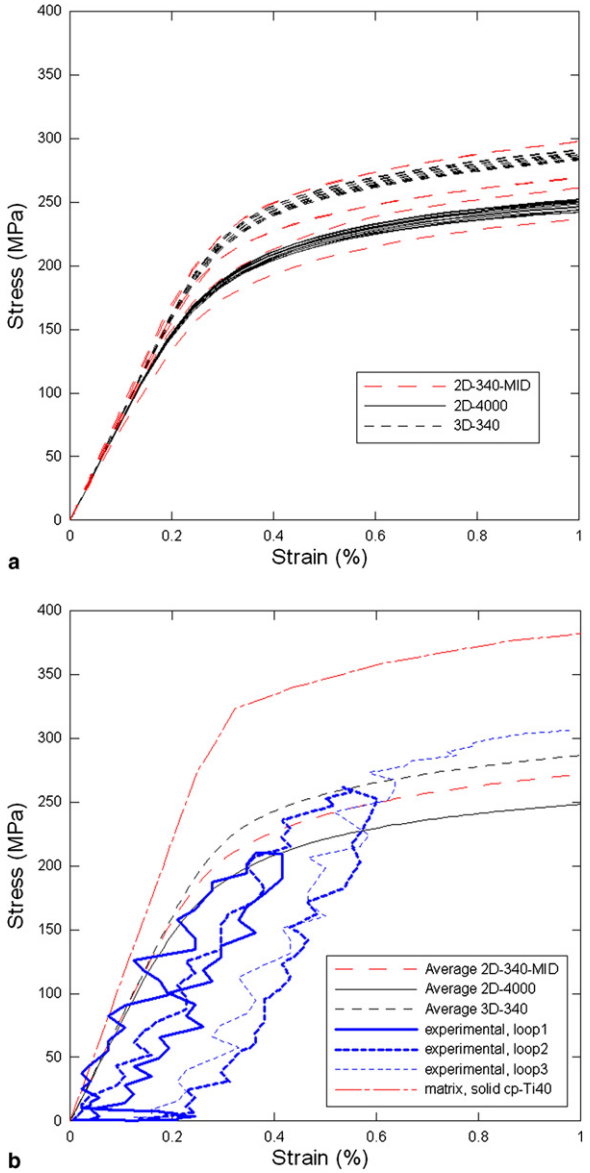

Fig. 5. Macroscopic stress–strain response of titanium foam obtained by (a) the 2D and 3D models and (b) a compressive test on a specimen of Ti foam at 15% porosity and the 2D and 3D models for comparison. Response of solid CP-Ti is shown for reference.

Table 2
The predictions for elastic modulus, 0.2% offset yield strength, and overall stress in uniaxial loading direction at 1% uniaxial strain by the 2D and 3D FE models

	E (GPa)		σ_y (MPa)		σ (MPa)	
	Avg ± sd	Max diff. (%)	Avg ± sd	Max diff. (%)	Avg ± sd	Max diff. (%)
2D-340 (individual)	81.37 ± 4.88	18.92	239.27 ± 23.32	29.91	271.81 ± 23.31	25.87
2D-4000 (individual)	78 ± 0.34	1.35	218.89 ± 2.85	3.97	248.15 ± 3.58	4.31
3D-340 (individual)	81.42 ± 0.63	2.3	257.92 ± 2.87	3.28	286.66 ± 2.75	2.91

2D and 3D models. The constitutive stress–strain response for the titanium matrix is also shown for reference. There were two loading and unloading loops before the specimen was loaded to a high strain. Strain

accumulation can be observed upon unloading at the end of the second loop in which plastic strain was localized in the porous microstructure.

The 3D FE models predicted Young's modulus of 81.4 GPa and the 0.2% offset yield strength of 258 MPa on average. For comparison, the analytical prediction of Young's modulus based on Mori–Tanaka theory is 81.79 GPa (Aboudi, 1991). Based on the experiment, Young's modulus was found to be 78 GPa by fitting the loading curve below 100 MPa of the first loop. The 0.2% offset yield strength of the material is roughly 261 MPa. The predicted macroscopic responses from the 3D model are in reasonable agreement with the experimental and theoretical results. While the plastic responses predicted by 2D-4000 models are lower than the experimental response, the elastic modulus prediction agrees well with the experimental and theoretical results. However, it should be noted that only one sample was used for the experiment and it was reported by Davis et al. (2001) that there can be large scatter in experimental results for porous metals (Davis et al., 2001).

3.2. Microscopic response

The Von Mises stress distributions computed by Eqs. (2)–(4) in the matrices of the 2D and 3D models deformed in perpendicular directions are plotted in Fig. 6. The distributions of the Von Mises stress in the 3D models are narrower than in the 2D models indicating the more uniform distributions in the 3D models. The range of the mean values of the 3D-340 models is 1.34% which is smaller than 4.16% for the 2D-4000 models and 13.43% for the 2D-340-MID models. The 3D models predict a mean Von Mises stress 21.04% higher than the 2D-4000 models. Although not shown here, similar trends were found for the equivalent plastic strain distributions for all the model groups.

Since the failure of the material follows a weakest link progression, failure is more likely to happen in models with a higher probability of the stress and strain exceeding a high value. Therefore, the accumulative frequencies of the Von Mises stress and equivalent plastic strain of the 2D and 3D models are plotted in Figs. 7 and 8. They were obtained by calculating the percentage of all the matrix elements exceeding a certain value in each model group. For Von Mises stress distribution, as is evident in Fig. 7, the 2D models predict higher probability than the 3D models at stress beyond 390 MPa. The frequency curve predicted by the three 2D-340-MID models shows that about 17% of the entire matrix in the models remains unloaded and the probability of stress beyond 390 MPa is lower than the other 2D-4000 models due to the bias produced by models smaller than RVEs. For equivalent plastic strain distribution, Fig. 8 shows that the 2D models predict higher probability than the 3D models at strain beyond 0.01. Since local plastic strain is critical for void nucleation

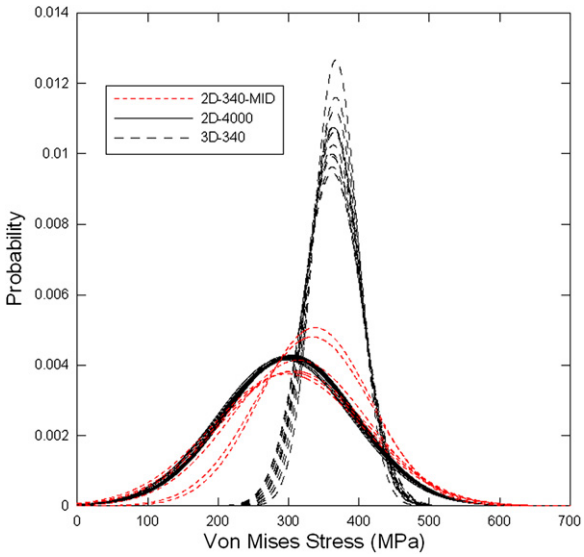

Fig. 6. Distributions of the Von Mises stress at 1% macroscopic strain predicted by the 2D and 3D FE models.

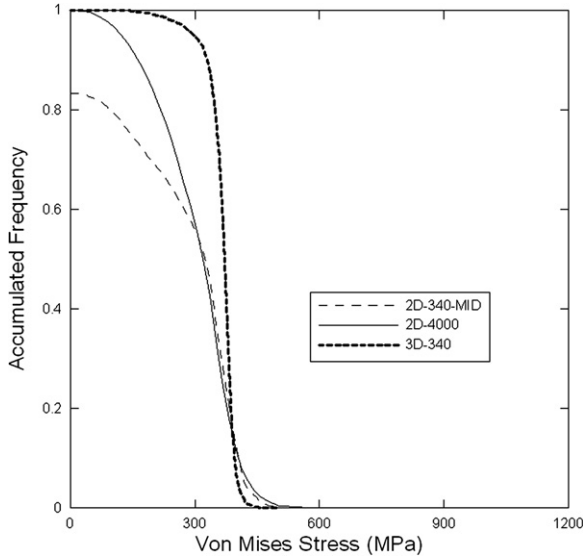

Fig. 7. Probabilities of the Von Mises stresses at 1% macroscopic strain in the 2D and 3D model groups exceeding a certain value.

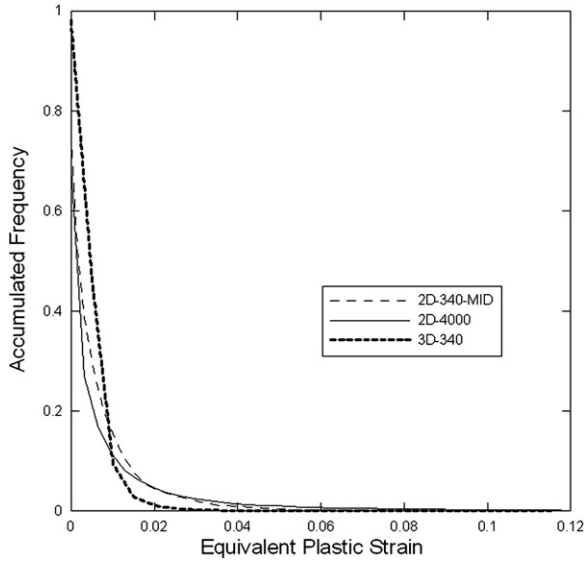

Fig. 8. Probabilities of the equivalent plastic strains at 1% macroscopic strain in the 2D and 3D model groups exceeding a certain value.

and growth leading to ductile fracture in the matrix, the 2D models are likely to overestimate the probability of matrix failure. While almost all matrix elements yield in 3D models under the loading of 1% compressive strain, approximately 30% of the matrix in the 2D models still remains elastic.

To get a clear comparison of the Von Mises stress distributions in the 2D and 3D models, the Von Mises stress distributions predicted by the 2D-340 models and the 3D-340 model at the corresponding sections are shown in Figs. 9–11. As shown in the 2D models, as porosity increases from 4.4% to 29.2%, Von Mises stress distribution patterns change from relatively uniform distribution in the range of 300–400 MPa to the distribution localized into obvious bands. These localized bands connect most pores while most regions remain at stress value lower than 300 MPa. Although the 3D-340 model also predicts stress localization near pores,

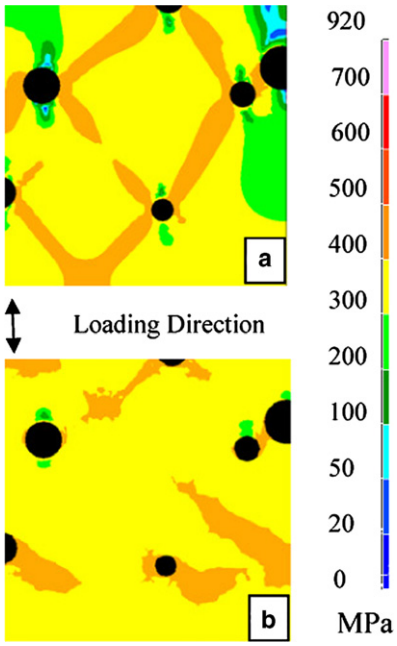

Fig. 9. Von Mises stress distribution at 1% macroscopic strain predicted by (a) the 2D-340-MIN and (b) the corresponding 3D-340 model.

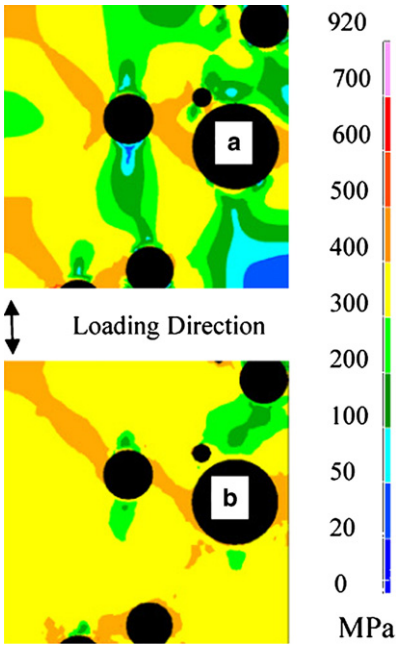

Fig. 10. Von Mises stress distribution at 1% macroscopic strain predicted by (a) the 2D-340-MID and (b) the corresponding 3D-340 model.

the Von Mises stress is relative uniformly distributed around 300–400 MPa for all the corresponding sections with porosity 4.4%, 14.7%, and 29.2%. These observations imply that under strain controlled loading condition, the higher the porosity is, the lower the overall stress and more localized stress distribution for 2D model. Therefore, more differences can be found for stress distribution at high porosity sections between 2D and 3D model.

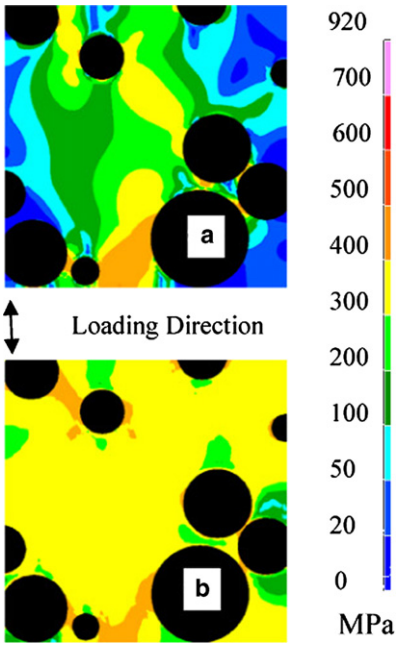

Fig. 11. Von Mises stress distribution at 1% macroscopic strain predicted by (a) the 2D-340-MAX and (b) the corresponding 3D-340 model.

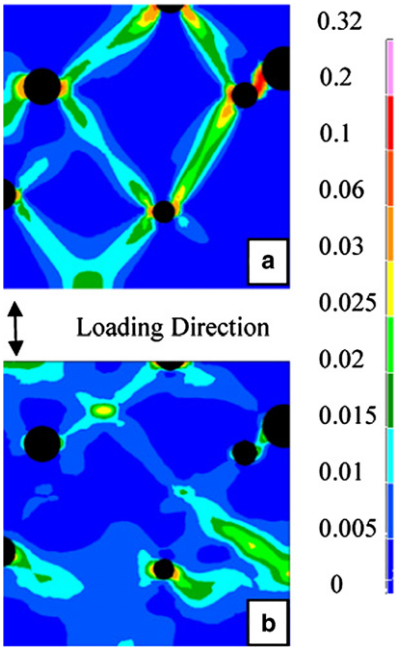

Fig. 12. Equivalent plastic strain distribution at 1% macroscopic strain predicted by (a) the 2D-340-MIN and (b) the corresponding 3D-340 model.

Figs. 12–14 directly compare the equivalent plastic strain distributions predicted by models 2D-340-MIN, 2D-340-MID, and 2D-340-MAX with the distributions obtained by the 3D-340 model at the corresponding sections. The 2D-340-MIN model in Fig. 12(a) predicts the plastic strain localized into distinct net-worked bands that connect all pores. While in Fig. 12(b) the 3D model also predicts localized plastic strain, no band

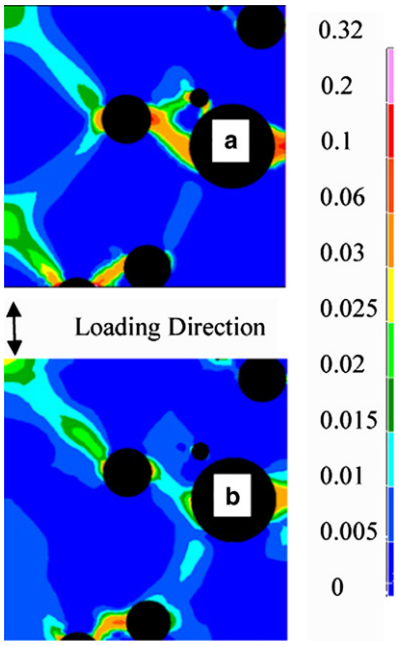

Fig. 13. Equivalent plastic strain distribution at 1% macroscopic strain predicted by (a) the 2D-340-MID and (b) the corresponding 3D-340 model.

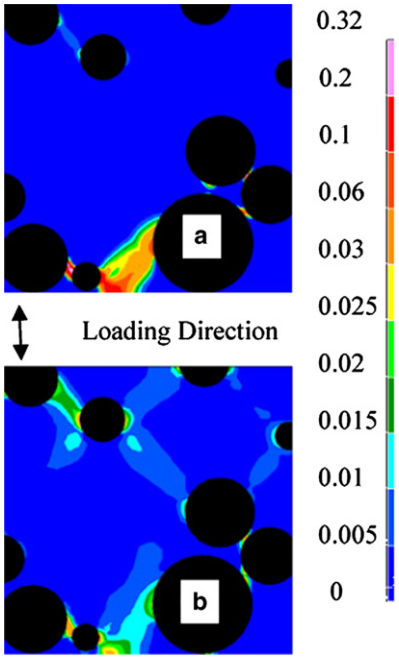

Fig. 14. Equivalent plastic strain distribution at 1% macroscopic strain predicted by (a) the 2D-340-MAX and (b) the corresponding 3D-340 model.

network is observed. As the pore area fraction of 2D model matches the porosity of 14.7% as shown in Fig. 13(a), although the plastic strain bands are more intensive than the corresponding 3D model in Fig. 13(b), the pattern of the bands becomes similar. As the area fraction increases to 29.2% in Fig. 14, a

dominant plastic band connects the horizontally closely spaced pores in the bottom region to form a "weak zone" for both the 2D and 3D models. It seems that the compressive deformation of the model is all absorbed by the "weak zone" in the 2D model and the other region of the model is therefore "unloaded". Although a plastic band can be observed in the same region in the corresponding 3D model, it is not as intensive as in the 2D model since the 3D analysis takes into account the geometry information out of the plane and the deformation is correspondingly spread more evenly through the model.

The more intensive localization of stress and strain explains why large 2D models are needed to get the same level of converged macroscopic response compared to smaller 3D models. In contrast to results for PR MMCs where differences between 2D models and the corresponding sections in 3D models are magnified as the particle area fraction increases (Shen and Lissenden, 2002), for the porous metal structures here similarities in the plastic strain distribution pattern between 2D model and the corresponding sections in 3D models increase as the pore area fraction increase. This result can be explained by noting that as inclusion area fraction increases in PR MMCs there is less matrix material capable of deforming plastically, while in a porous material there is more pore volume with zero modulus which is easy to deform.

4. Conclusions

Two groups of 2D models and one group of 3D models have been constructed based on a simulated microstructure of a porous material of low ($\sim$15%) porosity. The results led us to the following conclusions.

The predicted macroscopic responses from the 3D models are in reasonable agreement with the experimental and theoretical results. The macroscopic plastic responses predicted by 2D models are lower than the experimental result while the elastic responses are close to experimental and theoretical results. Window sizes of 2D models need to be larger than 3D models to obtain relatively convergent predictions. This implies 2D FE analysis on porous metals needs larger RVEs. For microscopic response, the 3D models predict higher mean Von Mises stress and equivalent plastic strain than 2D models but relatively uniform distributions. Thus, even though average stresses are lower, the 2D models overpredict the probability of high Von Mises stresses and equivalent plastic strains. This result is attributed to the more intensive localized deformation in 2D models as supporting material surrounding the plane section is not considered. Not surprisingly, the highest strain localizations occur in regions where the pores closely spaced in the direction perpendicular to the loading direction. As the area fraction of pores increases, more similarities can be found in the strain distribution patterns between 2D and 3D models.

In high porosity foams, "weak zones" are likely to form between closely spaced pores, linked in the direction perpendicular to loading direction in 2D model. As in the results here, the "weak zones" will attract high strain localization and will unload portions of the model leading to lower macroscopic stress than 3D model prediction. While modeling higher porosity foams is a challenge, particularly in terms of obtaining an appropriate RVE, the results here indicate further work should be done in this area rather than rely on 2D simulations.

While 2D micrographs can be more readily obtained and easily examined in FE analysis, information on 2D sections differs significantly from 3D analyses as shown here. The discrepancies do not preclude the possible use of 2D models where it may be considered "good enough" to observe the nonuniform strain distribution pattern or as a tool to guide choice between specific larger scale features, such as overall porosity. However, a 3D model is necessary to predict both macroscopic and microscopic responses and is especially essential for the design of microstructural architecture, where the goal is to optimize the pore size and location distribution. As the initial pore size and location distribution depends on the size distribution and arrangement of the sieved powders, some processing parameters can be altered to obtain a desired 3D foamed microstructure based upon accurate simulations.

Acknowledgements

The authors acknowledge the financial support of the National Science Foundation through grant number DMR-0505772 as well as the help and support from Professor David C. Dunand and Scott M. Oppenheimer in the Materials Science and Engineering Department at Northwestern University.

References

Aboudi, J., 1991. Mechanics of composite materials—a unified micromechanical approach. Elsevier Science Publishing Company, Inc.

ASM International, 2002. Atlas of Stress–strain Curves, second ed. ASM International, Materials Park, OH.

Benveniste, Y., 1987. A new approach to the application of Mori–Tanaka's theory in composite materials. Mech. Mater. 6, 147–157.

Bohm, H.J., Han, W., 2001. Comparison between three-dimensional and two-dimensional multi-particle unit cell models for particle reinforced metal matrix composites. Model. Simul. Mater. Sci. Eng. 9, 47–65.

Bohm, H.J., Eckschlager, A., Han, W., 2002. Multi-inclusion unit cell models for metal matrix composites with randomly oriented discontinuous reinforcements. Comput. Mater. Sci. 25, 42–53.

Bouyge, F., Jasiuk, I., Ostoja-Starzewski, M., 2001. A micromechanically based couple-stress model of an elastic two-phase composite. Int. J. Solids Struct. 38, 1721–1735.

Bouyge, F., Jasiuk, I., Boccara, S., Ostoja-Starzewski, M., 2002. A micromechanically based couple-stress model of an elastic orthotropic two-phase composite. Eur. J. Mech. A—Solids 21, 465–481.

Chang, Y-S., Oka, M., Kobayashi, M., Gu, H-O., Li, Z-L., Nakamura, T., Ikada, Y., 1996. Significance of interstitial bone ingrowth under load-bearing conditions: a comparison between solid and porous implant materials. Biomaterials 17, 1141–1148.

Christman, T., Needleman, A., Suresh, S., 1989. An experimental and numerical study of deformation in metal–ceramic composites. Acta Metall. 137, 3029–3050.

Davis, N.G., Teisen, J., Schuh, C., Dunand, D.C., 2001. Solid-state foaming of titanium by superplastic expansion of argon-filled pores. J. Mater. Res. 16 (5), 1508–1519.

Daxner, T., Bohm, H.J., Rammerstorfer, F.G., Denzer, R., Maier, M., 2000. Simulation of elastic–plastic behavior of metal foam using 2D and 3D unit cell models. Mater. Wiss. Werkstofftechnik 31, 447–450.

Dunand, D.C., 2004. Processing of titanium foams. Adv. Eng. Mater. 6 (6), 369–376.

Ghosh, S., Lee, K., Moorthy, S., 1996. Two scale analysis of heterogeneous elastic–plastic materials with asymptotic homogenization and Voronoi cell finite element model. Comput. Methods Appl. Mech. Eng. 132, 63–116.

Gibson, L., Ashby, M., 1997. Cellular Solids: Structure and Properties. Cambridge University Press.

Hazanov, S., 1999. On apparent properties of nonlinear heterogeneous bodies smaller than the representative volume. Acta Mech. 134, 123–134.

Hibbitt Karlsson Sorensen Inc., 2004. ABAQUS Ver. 6-4 Standard User's Manual.

Huet, C., 1990. Application of variational concepts to size effects in elastic heterogeneous bodies. J. Mech. Phys. Solids 38 (6), 813–841.

Jiang, M., Ostoja-Starzewski, M., Jasiuk, I., 2001. Scale-dependent bounds on effective elastoplastic response of random composites. J. Mech. Phys. Solids 49, 655–673.

Ju, J.W., Tseng, K.H., 1996. Effective elastoplastic behavior of two-phase ductile matrix composites: a micromechanical framework. Int. J. Solids Struct. 33, 4267–4291.

Li, H., Oppenheimer, S.M., Stupp, S.I., Dunand, D.C., Brinson, L.C., 2004. Effects of pore morphology and bone ingrowth on mechanical properties of microporous titanium as an orthopaedic implant material. Mater. Trans. 45 (4), 1124–1131.

Lissenden, C.J., Shen, H., 2001. Finite element modeling of discontinuously reinforced aluminum in 2D and 3D. In: Pandey, A.B., Kendig, K.L., Watson, T.J. (Eds.), Affordable Metal–Matrix Composites for High Performance Applications. The Minerals, Metals, and Materials Society, Warrendale, OH.

Llorca, J., Needleman, A., Suresh, S., 1991. An analysis of the effects of matrix void growth on deformation and ductility in metal–ceramic composites. Acta. Metall. Mater. 39, 2317–2335.

Mori, T., Tanaka, K., 1973. Average stress in matrix and average elastic energy of materials with misfitting inclusions. Acta Metall. 21, 571–574.

Murray, N.G.D., Dunand, D.C., 2003. Microstructure evolution during solid-state foaming of titanium. Compos. Sci. Technol. 63, 2311–2316.

Ochsner, A., Lamprecht, K., 2003. On the uniaxial compression behavior of regular shaped cellular metals. Mech. Res. Commun. 30, 573–579.

Ramakrishnan, N., Kumar, A.M., Radhakrishna Bhat, B.V., 1996. A generalized plane strain technique for estimating effective properties of particulate metal matrix composites using FEM. J. Mater. Sci. 31, 3507–3512.

Shen, H., Brinson, L.C., in press. A numerical investigation of the effect of boundary conditions and RVE size on simulation of foamed titanium. J. Mech. Mater. Struct.

Shen, H., Brinson, L.C., in preparation. A numerical investigation of titanium foam as orthopedic implant material.

Shen, H., Lissenden, C.J., 2002. 3D finite element analysis of particle-reinforced aluminum. Mater. Sci. Eng. A 338, 271–281.

Shen, H., Lissenden, C.J., 2005. Stress and strain localization three-dimensional modeling for particle-reinforced metal matrix composites. Metall. Mater. Trans. A 36A, 1653–1660.

Shen, H., Oppenheimer, S.M., Dunand, D.C., Brinson, L.C., 2006. Numerical modeling of pore size and distribution in foamed titanium. Mech. Mater. 38, 933–944.

Sihn, S., Roy, A.K., 2004. Modeling and prediction of bulk properties of open-cell carbon foam. J. Mech. Phys. Solids 52, 167–191.

Simone, A.E., Gibson, L.J., 1998. Effects of solid distribution on the stiffness and strength of metallic foams. Acta Mater. 46 (6), 2139–2150.

Song, S.G., Shi, N., Gray III, G.T., Roberts, J.A., 1996. Reinforcement shape effects on the fracture behavior and ductility of particulate-reinforced 6061-Al matrix composites. Metall. Mater. Trans. A 27A, 3739–3746.

Spoerke, E.D., Murray, N.G., Li, H., Brinson, L.C., Dunand, D.C., Stupp, S.I., in press. A bioactive titanium foam scaffold for bone repair. Acta Biomater.

Thelen, S., Barthelat, F., Brinson, L.C., 2004. Mechanics considerations for microporous titanium as an orthopaedic implant material. J. Bio. Mater. Res. A 69, 601–610.

Tobias, P.A., Trindade, D.C., 1995. Appl. Reliab., 81–104.

Wang, Z., Chen, T.-K., Lloyd, D.J., 1993. Stress distribution in particulate-reinforced metal-matrix composites subjected to external load. Metall. Trans. A 24, 197–207.

Weissenbek, E., Bohm, H.J., Rammerstorfer, F.G., 1994. Micromechanical investigation of arrangement effects in particle reinforced metal matrix composites. Comput. Mater. Sci. 13, 263–278.

Wen, C.E., Yamada, Y., Shimojima, K., Chino, Y., Asahina, T., Mabuchi, M., 2002a. Processing and mechanical properties of autogenous titanium implant materials. J. Mater. Sci.: Mater. Med. 13, 397–401.

Wen, C.E., Yamada, Y., Shimojima, K., Chino, Y., Hosokawa, T., Mabuchi, M., 2002b. Novel titanium foam for bone tissue engineering. J. Mater. Res. 17 (10), 2633–2639.

Wolodko, J.D., Xia, Z., Ellyin, F., 2000. Analysis of A/Al_2O_3 metal matrix composites under biaxial cyclic loading using a digital image based finite element method. Mater. Sci. Technol. 16, 837–842.